JOURNAL OF MATERIALS SCIENCE 19 (1984) 1145–1152

Mechanism of fracture of short glass fibre-reinforced polyamide thermoplastic

NORIO SATO, TOSHIO KURAUCHI, SHIGEYUKI SATO, OSAMI KAMIGAITO
Toyota Central Research and Development Laboratories, Inc., Nagakute-cho, Aichi-gun, Aichi, 480-11, Japan

The mechanism of fracture of short glass fibre-reinforced polyamide 6.6 thermoplastic was studied by means of optical and electron microscopy and acoustic emission methods. It was found that there were three stages in the failure, i.e. initiation of the interfacial cracks at fibre ends, propagation of the interfacial cracks along fibre sides, and propagation of the crack into the matrix leading to the failure of the composite. On the fracture surface, fibres were almost pulled-out from the matrix, not broken. The close correspondence between the crack initiation and propagation and the amplitude of AE signals was observed. The AE signals of lower amplitude occurring under a relatively low stress were considered to be made in association with the initiation and propagation of the interfacial cracks. The AE signals of higher amplitude observed prior to the failure of the composite were considered to be made in association with the occurrence of the matrix cracks. Furthermore, in order to analyse the effect of the stress state in the composite on crack occurrence and propagation, the stress levels in matrix, fibre and interface were estimated for the composite stressed to the failure stress. The calculation was based on the equivalent inclusion method proposed by Eshelby and on an assumption of a perfect bond between the matrix and the fibres. The result was found to be consistent with the mechanism of the fracture, the occurrence of the interfacial cracking in the initial stage and the matrix cracking in the final one.

1. Introduction

Short fibre-reinforced thermoplastics are being applied to automobiles because of their ease of fabrication, their light weight, and economy. For example, timing gears, radiator fans, radiator tanks and box structures are now made of short glass fibre-reinforced thermoplastics. For these applications, high reliability of components is required. And the investigation of the mechanism of the fracture of the composite is very important to prove the reliability of the components. The mechanism of the fracture of the composite, however, seems not to have been fully clarified because of the complicated behaviour of the failure, which is much affected by the fibre length, the fibre orientation and the fibre/matrix bond strength, etc. Several theoretical studies of the composite strength have been made on the basis of various postulated fracture mechanisms. For example, Riley [1] investigated the strength by modifying the formula of linear superposition of the strength of each component in the composite, and showed that the failure will initiate when fibre stress reaches the ultimate tensile strength. Fukuda and Chou [2] made a probabilistic approach to the failure, taking account of the fibre failure caused under the influence of the neighbouring fibre end. Taya [3] has studied the strength of a composite whose failure is initiated by penny-shaped cracks in the matrix. Curtis *et al.* [4] made an experimental study and showed that the occurrence and accumulation of cracks at fibre ends greatly affect the mechanical behaviour of the composite. In these studies, however, detailed investigations have

0022–2461/84 $03.00 + .12

not been made of individual failure processes such as crack initiation, propagation and breakdown. Detailed information of their processes is thought to be important for the clarification of the failure mechanism of the composite.

In the present work, experiments and theoretical analysis have been made to investigate the mechanism of the fracture of a short glass fibre-reinforced thermoplastic composite. First, as a non-destructive method, an acoustic emission monitoring system was used to detect the initiation and propagation of the cracks and to separate different failure mechanisms. Second, the specimen surface under stress and the fracture surface were observed with an optical microscope and a scanning electron microscope. Third, the stress level in each constituent of the composite subjected to the failure stress was calculated on the basis of Eshelby's theory [5]. On the consideration of these results, a mechanism of fracture of the composite was postulated.

2. Experimental detail

Thermoplastic polyamide 6.6 reinforced with short glass fibres was prepared for the study. Polyamide 6.6 pellets and glass fibres were purchased from Asahi Chemical Industry Co. Ltd. and Nipon Glass-fibre Co. Ltd., respectively. The glass fibres were treated with a coupling agent of γ-aminopropyltrimethoxysilane and a film forming agent before mixing with the polyamide. The pellets and the glass fibres were compounded in an extruder and then injection moulded into the tensile test specimen at the temperature of 280° C. The dimension of the tensile test specimen was selected to confirm the specification of ASTM D638. The gate of the mould was located at the end of the specimen, and the molten resin flowed along the longitudinal axis of the specimen on moulding. Thus the short fibres embedded in the matrix were aligned along the flow direction. The volume fraction of fibres in the specimen was in the range from 0.026 to 0.25. The mean diameter and length of the fibres were about 13 and 400 μm, respectively, and therefore the aspect ratio was about 30. The moulded specimen was kept in a desiccator with the humidity at about 20% until testing.

The specimen was submitted to a tensile test at room temperature on an Instron-type machine. The stress–strain curve and the fracture stress of the specimen was obtained at the strain rate of $1.7 \times 10^{-4}\,\mathrm{sec}^{-1}$. The test was made under an acoustic emission monitoring by the use of the system, Dunegan/Endevco 3000 series. Two methods of data analysis were applied to characterize the acoustic emission from the composite. One is a ring down count method. During the tensile test, all AE signals detected by the sensor (resonant peak at 140 kHz) are submitted to highpass-filter (100 kHz) and amplified with a preamplifier and a main amplifier. The total system amplification is maintained at 80 dB. The digital counter is adjusted to count only the amplified emission signal which exceeds a threshold value (1 V). By this method, the time and the rate of crack occurrence were detected. The other is an amplitude distribution analysis method. All signals amplified with the preamplifier (40 dB) are sorted according to the value of the maximum amplitude, and the population of the signal is plotted against the maximum amplitude (amplitude spectrum). In the spectrum, the amplitude is adjusted to range from 0 to 100 dB. Using this method, the different failure origins involved in the composite were detected.

In order to observe the crack initiation and propagation in the specimen, the polished surface of the specimen under stress or after failure was examined by an optical microscope. The scanning electron microscope was also used to observe the fracture surface of the specimen.

3. Results

3.1. Acoustic emission

Fig. 1 shows a typical example of AE signals obtained from a specimen with 0.16 volume fraction of fibres. The stress–strain curve is also shown in the same figure. Acoustic emission begins at a low level of about one fourth of the maximum load and increases remarkably with the elevated load.

Fig. 2 shows the result of the amplitude distribution analysis for various levels of loading up to the specimen failure. In the spectrum, a population peak is observed at the amplitude of 51 dB for the load ranging from 60% to 80% and that ranging from 80% to 90% of the maximum load. Under the load ranging from 90% to 95% of the maximum, signals of much higher amplitude (63 dB) accompanied with those of lower amplitude were observed. Under the maximum load, only signals of the higher amplitude were observed, which is in contrast to the presence of double peaks under the lower load.

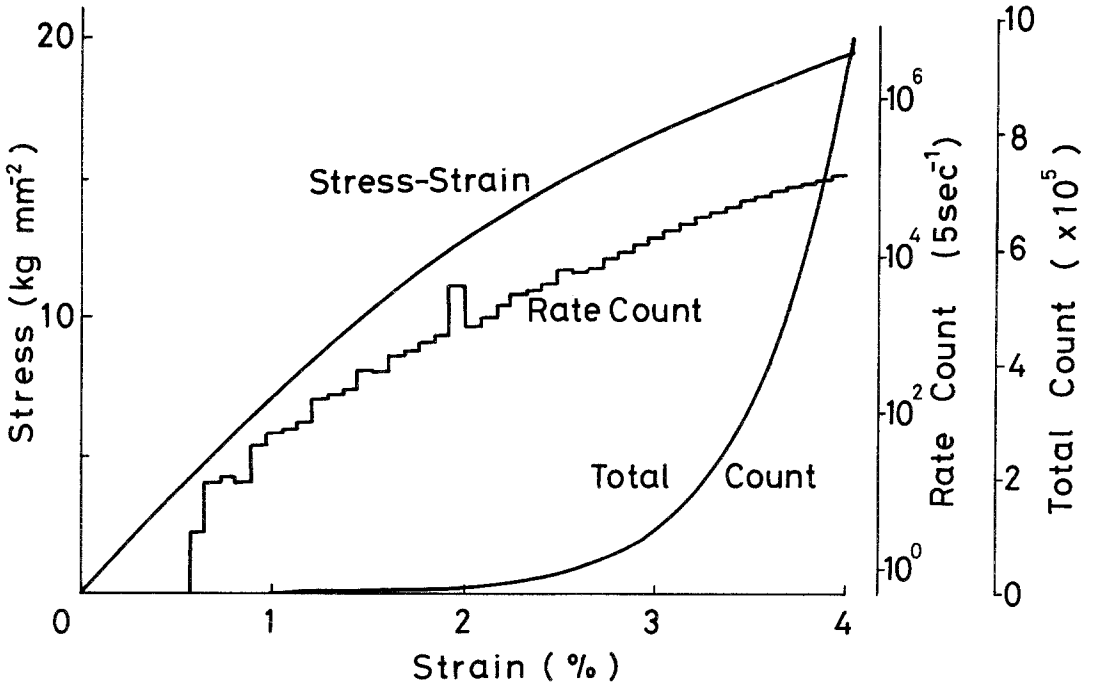

Figure 1 Tensile stress–strain curve of 16 vol% short glass fibre-reinforced polyamide composite and rate and total AE counts obtained at the tensile test.

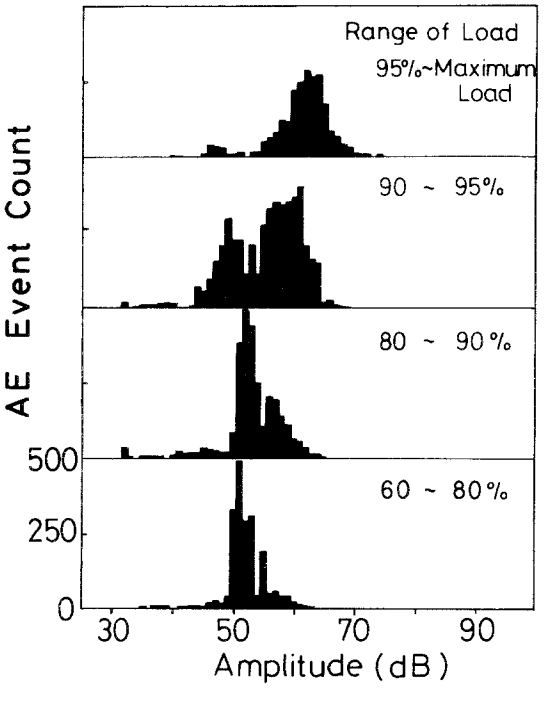

Figure 2 Amplitude distribution analysis of AE signals for various levels of loading up to the composite failure.

3.2. Microscopic observation

Fig. 3a shows a typical example of the surface of a specimen under one half of the maximum load. The initiation of an interfacial crack is observed at fibre end. As the load was increased, the interfacial crack was observed to propagate along the interface of the fibre sides. Fig. 3b shows the surface of the specimen unloaded after loading to 95% of the maximum load. The cracks were observed to propagate along the interface of the fibre sides and to extend from the interface to the matrix. After the failure, many matrix cracks were observed, particularly beneath the fracture surface (Fig. 3c). The matrix cracks were observed to initiate from the interfaces and propagate almost perpendicularly to the tensile direction. No fibre breakage was observed in the specimen.

Fig. 4 shows the fracture surface examined with SEM. Most of the fibre were pulled out and the surface of the fibre was observed to be covered with thin matrix films.

4. Stress analysis

4.1. Model and fundamental equations

In order to consider the mechanism of fracture, the stress levels in matrix, fibre and interface were

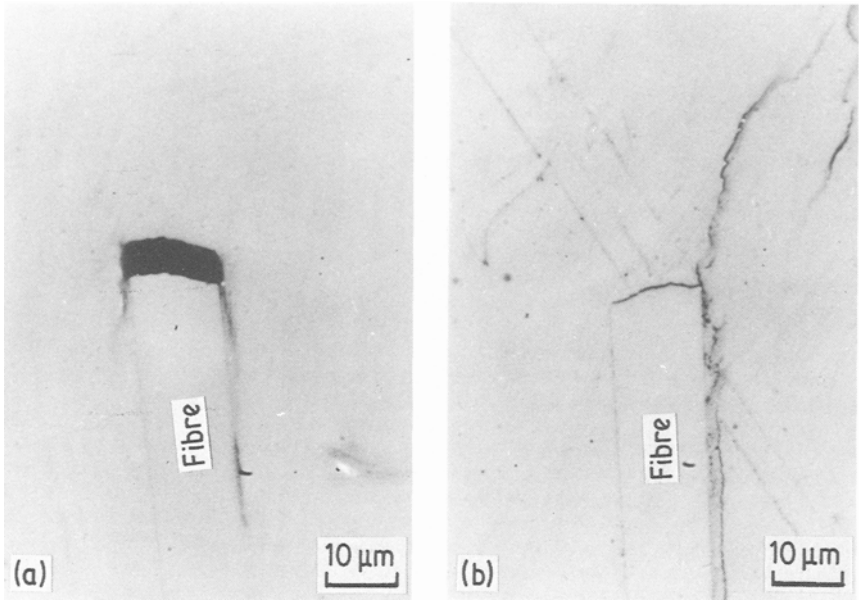

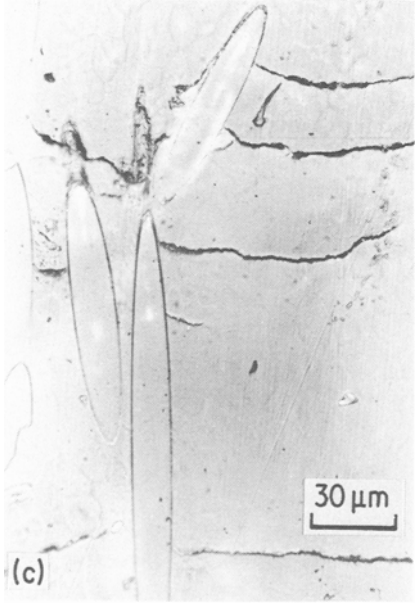

Figure 3 Initiation and propagation of crack. (a) Initiation of an interfacial crack at the fibre end observed on the surface of the composite under one half of the maximum load. (b) Propagation of the crack along the interface of the fibre sides and extention of the crack into the matrix observed on the surface of the composite unloaded after loading to 95% of the maximum load. (c) Propagation of the crack into the matrix observed beneath the fracture surface.

estimated for the composite submitted to the failure stress. The analysis was based on the equivalent inclusion method proposed by Eshelby [5] and Mori–Tanaka's back stress analysis [6]. The analysis was made on the model shown in Fig. 5a on the assumption that

1. the shape of the short fibre can be approximated by an ellipsoid,

2. all fibres are of uniform length, aligned in the loading direction and dispersed randomly in the composite specimen. The fibre axis agrees with x_3-axis of the Cartesian coordinates,

3. the matrix and fibres are perfectly bonded together at their interfaces,

4. the matrix and fibres are entirely elastic until the composite fails.

When a single short fibre is embedded in the matrix and the composite is submitted to the applied stress $\sigma_{ij}^{A}(i, j = 1, 2, 3)$, the stress in the fibre σ_{ij}^{F} can be calculated as follows [5],

$$\sigma_{ij}^{F} = \sigma_{ij}^{A} + \sigma_{ij}^{C} = C_{ijkl}^{*}(\epsilon_{kl}^{A} + \epsilon_{kl}^{C}) = C_{ijkl}(\epsilon_{kl}^{A} + \epsilon_{kl}^{C} - \epsilon_{kl}^{T}) \quad (1)$$

where C_{ijkl}^{*}, C_{ijkl} are elastic moduli of the fibre and the matrix, respectively, σ_{ij}^{C} and ϵ_{kl}^{C} are the disturbance of stress and strain due to the fibre. σ_{ij}^{A} and ϵ_{kl}^{A} are the uniform applied stress and strain,

$$\sigma_{ij}^{A} = C_{ijkl}\epsilon_{kl}^{A}. \quad (2)$$

In Equation 1, ϵ_{kl}^{T} is related to the disturbed strain ϵ_{ij}^{C} as,

$$\epsilon_{ij}^{C} = S_{ijkl}\epsilon_{kl}^{T} \quad (3)$$

where S_{ijkl} is Eshelby's tensor which is determined by the aspect ratio of the fibre and Poisson's ratio of the matrix.

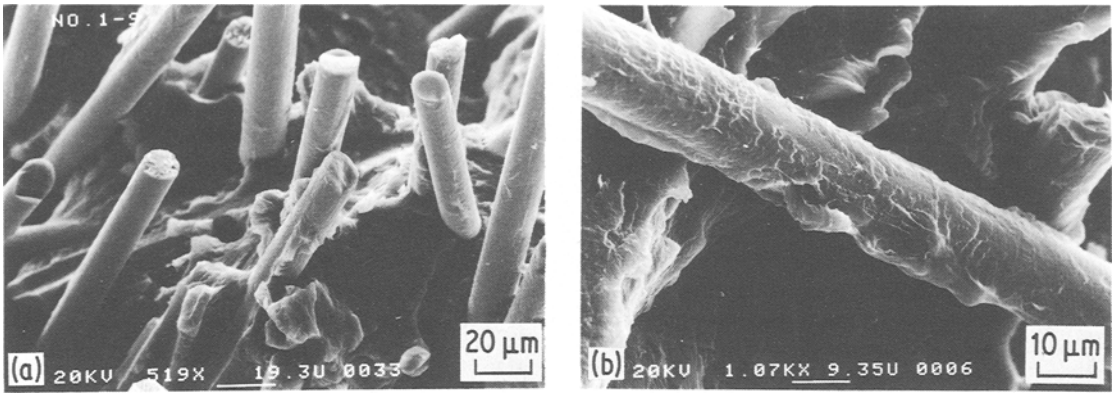

Figure 4 Fracture surface. (a) Overview of the fracture surface showing the pulled-out fibres. (b) Surface of the glass fibre showing being covered with thin matrix films.

When a large number of fibres are embedded in the matrix, it is necessary to take into account the effect of the interaction among the fibres. For this purpose, an approximate smearing-out method has been proposed by Mori and Tanaka [6] by introducing the image strain ϵ_{ij}^{im},

$$\epsilon_{ij}^{im} = -v(\epsilon_{ij}^{C} - \epsilon_{ij}^{T}) \quad (4)$$

where v is the volume fraction of fibres. Combination of these with Equation 1 gives the following,

$$\begin{aligned} \sigma_{ij}^{F} &= C_{ijkl}^{*}[\epsilon_{kl}^{A} + (1-v)\epsilon_{kl}^{C} + v\epsilon_{kl}^{T}] \\ &= C_{ijkl}[\epsilon_{kl}^{A} + (1-v)(\epsilon_{kl}^{C} - \epsilon_{kl}^{T})] \end{aligned} \quad (5)$$

Equation 5 is the first order simultaneous equation and the six components of the eigenstrain, ϵ_{ij}^{T}, can be obtained from the equation. The stress in the matrix σ_{ij}^{M} and in the fibre σ_{ij}^{F} can be obtained as follows [6, 7],

$$\sigma_{ij}^{M} = C_{ijkl}[\epsilon_{kl}^{A} - v(S_{klmn}\epsilon_{mn}^{T} - \epsilon_{kl}^{T})] \quad (6)$$

$$\sigma_{ij}^{F} = C_{ijkl}^{*}[\epsilon_{kl}^{A} + (1-v)S_{klmn}\epsilon_{mn}^{T} + v\epsilon_{kl}^{T}] \quad (7)$$

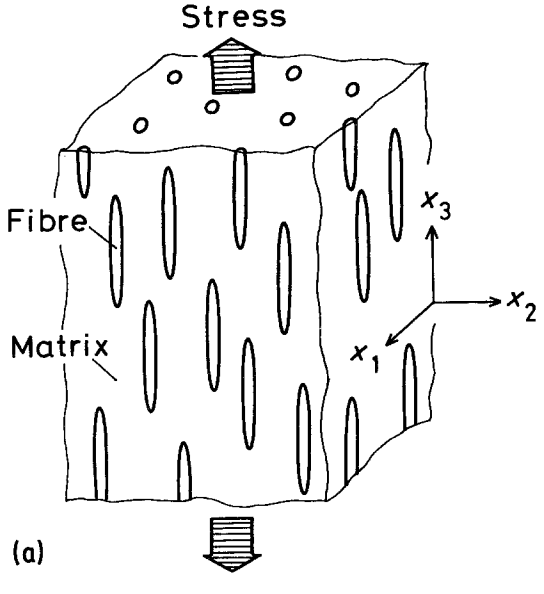

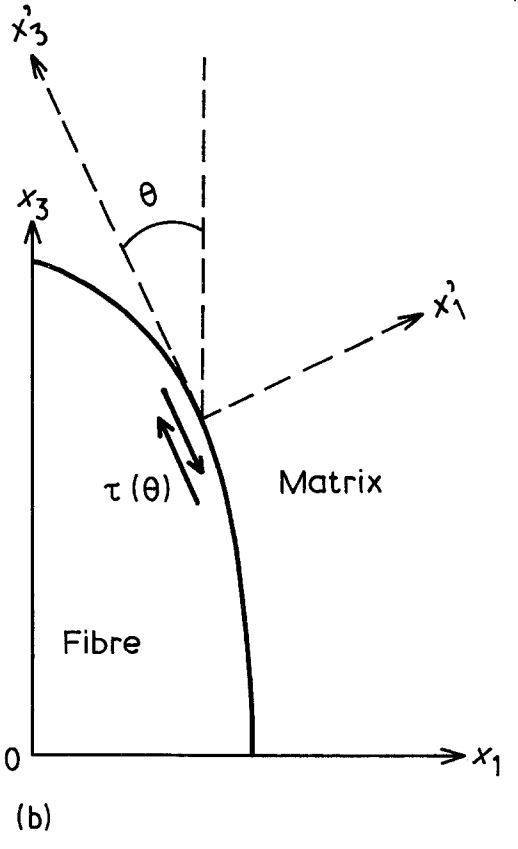

Figure 5 Calculation model. (a) Model of short fibre-reinforced composite. (b) Tangential shear stress at the elliptic fibre–matrix interface and the transformation of the coordinates.

The tangential shear stress at the elliptic interface (Fig. 5b) could be estimated from the stress in the fibre by an appropriate transformation of the coordinates. The tangential shear stress $\tau(\theta)$ at the interface due to the applied tensile stress is obtained by the following,

$$\tau(\theta) = \tfrac{1}{2}\sin 2\theta\{\sigma_{33}^{F} - \sigma_{11}^{F}\} \quad (8)$$

where σ_{33}^{F} and σ_{11}^{F} stand, respectively, for the longitudinal and transverse stress components in the fibre, and θ stands for the inclination angle of the interface against the loading direction. For $\theta = \pi/4$, the shear stress gives the maximum value, τ_{max},

$$\tau_{max} = \tfrac{1}{2}(\sigma_{33}^{F} - \sigma_{11}^{F}) \quad (9)$$

4.2. Results of calculation

The stress levels in the matrix, in the fibre and at the interface were calculated for the composite under the tensile fracture stress, $\sigma_{33}^{A} = \sigma_0$, where σ_0 is the tensile fracture stress of the composite which is determined through an experiment. The material constants used for the calculation are as follows,

Matrix; Young's modulus $E = 250\,\mathrm{kg\,mm^{-2}}$

Poisson's ratio $\nu = 0.4$

Fibre; Young's modulus $E^* = 7000\,\mathrm{kg\,mm^{-2}}$

Poisson's ratio $\nu^* = 0.23$

Aspect ratio of fibre; 30

Only σ_{33}^{M} and σ_{33}^{F} of the six stress components in both σ_{ij}^{M} and σ_{ij}^{F} were calculated because they are considered to affect much the composite fracture. The maximum shear stress at the interface was also calculated by Equation 9. The detail of the calculation is shown in the appendix.

The result of the calculation is shown in Table I for the composites of various volume fractions of fibres. The experimental tensile strength of the composite, σ_0, is also shown in the table.

TABLE I Tensile failure stress of the composite (σ_0) and calculated stress levels in matrix, in fibre and at interface at the composite failure

Failure stress of composite ($\mathrm{kg\,mm^{-2}}$)	Volume fration of fibre (%)	Calculated stress level ($\mathrm{kg\,mm^{-2}}$)		
		Matrix	Fibre	Interface
8.6	2.6	5.8	120	60
9.2	6.6	3.8	85	42
13.8	12.2	3.9	86	43
17.2	16.0	3.8	84	43
19.4	20.6	3.3	81	41
22.0	25.6	3.5	77	40

5. Discussion

The crack initiation and propagation of the short fibre-reinforced composite were observed by microscopy to occur as the following three processes: interfacial cracks occur at fibre ends, the cracks propagate along the interfaces of the fibre sides and finally the matrix cracks occur leading to the composite failure. The interfacial cracks in the first and second processes are formed in the matrix near the fibre sides and it is not due to the fibre/matrix interface debonding, as the surfaces of fibres are covered with thin film made of the resin. These cracks are considered to occur at a relatively low load and propagate as the load increases, because AE begins at the load of about one fourth of the maximum load and increased remarkably near the maximum load (Fig. 1).

From the comparison of AE data with the observation of the crack occurrence at a common load, AE signals can be related to the crack occurrence. The AE signals occurring at a relatively low load are considered to be due to the initiation of cracks at the fibre ends. The slight increment in the number of the signals with that in the load may be related to the crack propagation along the fibre sides. The remarkable increment in the number of the signals near the maximum load is considered to be related to the initiation of both interfacial cracks and matrix cracks. These AE signals are separated clearly according to their AE amplitude (Fig. 2). The signals of lower amplitude observed below 95% of the maximum load are considered to correspond to the occurrence of the interfacial damage shown in Figs. 3a and b. Those of higher amplitude observed prior to the failure are considered to correspond to that of the matrix shown in Fig. 3c.

From the stress analysis, an interesting fact emerged. As shown in Table I, stress levels of the matrix, the fibre and the interface just prior to the composite failure are almost constant in a wide range of the volume fraction of fibres. The stress level of the matrix just prior to the composite failure is nearly equal to the yield stress of unfilled polyamide 6.6 ($5.6\,\mathrm{kg\,mm^{-2}}$). The stress level of fibre is about one half of the fibre strength ($200\,\mathrm{kg\,mm^{-2}}$). The maximum shear stress of the interface is several times larger than the fibre/matrix shear bond strength ($6.5\,\mathrm{kg\,mm^{-2}}$ [4]). These

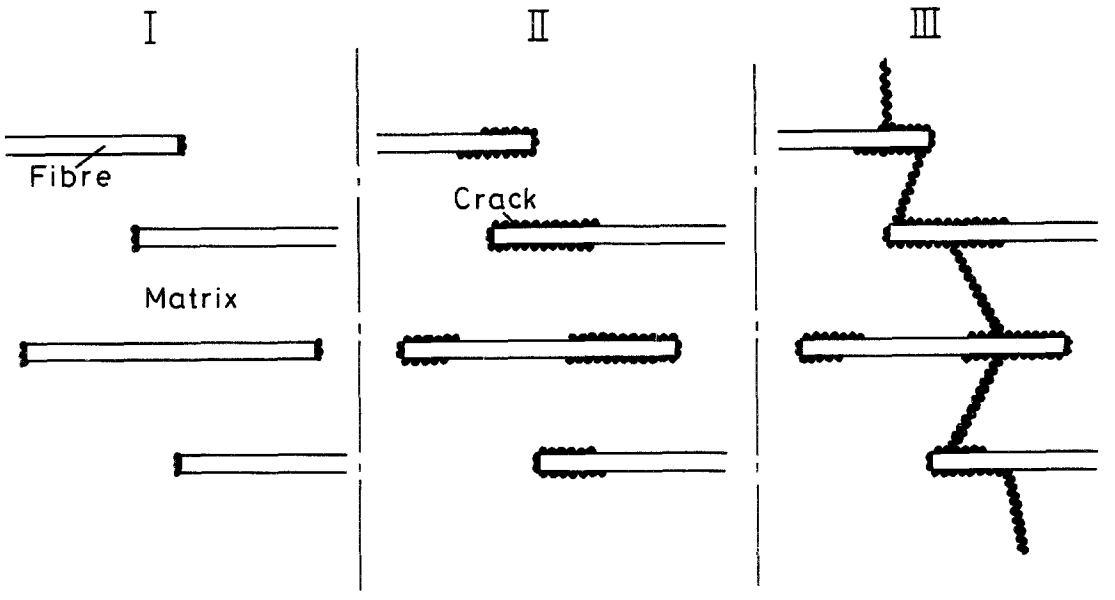

Figure 6 Model of mechanism of fracture. (I) First stage; occurrence of crack at fibre ends. (II) Second stage; propagation of the crack along the fibre sides. (III) Final stage; occurrence of the crack in the matrix.

results confirms the presumption that the interfacial crack will initiate under a relatively low load and the matrix crack will occur near the maximum load. No fibre breakage is considered to occur even at the maximum load. The occurrence of the matrix cracking without the large matrix yielding is considered to be attributed to the suppression of the matrix flow by the adjacent fibres. These theoretical indications are considered to be consistent with the initial fracture mechanism. The stress redistribution due to the debonding should be taken account of in order to estimate the stress state after the debonding as observed in the experiments.

The following mechanism of the fracture of the composite as shown in Fig. 6 can be proposed from the experimental and theoretical investigations. Under a load, the stress concentration occurs in the vicinity of fibres, especially at the fibre ends. Under the influence of the concentrated stress, cracks may occur at the fibre ends. This is the first stage of the failure. While, the shear deformation of the matrix along the fibre sides increases with stress. The interfacial cracks propagate from the fibre ends along the fibre sides due to the shear deformation of the matrix. This is the second stage of the failure. Due to the occurrence of these cracks, the load bearing capability of the fibres is much reduced, and the matrix is required to support a much more load. The matrix cracks come to grow from the interfacial cracks just prior to the composite failure. These interfacial cracks and matrix cracks may result in a catastrophic crack propagation leading to the composite failure. This is the final stage of the failure. Even in this stage, fibres are only pulled out from the matrix without being broken. This mechanism of fracture may explain the brittle manner of the composite failure, in contrast to the ductility of the unfilled polymer.

6. Conclusion

The mechanism of fracture of a short glass fibre-reinforced composite is postulated as follows; in the first stage the interfacial crack occurs at the fibre end, in the second stage the interfacial crack propagates along the fibre sides, and in the final stage the crack propagates in the matrix. Moreover, AE method and the theoretical analysis used in this study are considered to be useful for the study of the mechanisms of fracture of other short fibre-reinforced composites.

Appendix

The stresses in matrix σ_{33}^{M}, and in fibre σ_{11}^{F} and σ_{33}^{F} were given as follows,

$$\sigma_{33}^{M} = 2C_{3311}(\epsilon_{11}^{A} + \epsilon_{11}^{im}) + C_{3333}(\epsilon_{33}^{A} + \epsilon_{33}^{im})$$

$$\sigma_{11}^{F} = (C_{1111}^{*} + C_{1122}^{*})(\epsilon_{11}^{A} + \epsilon_{11}^{C} + \epsilon_{11}^{im}) + C_{2233}^{*}(\epsilon_{33}^{A} + \epsilon_{33}^{C} + \epsilon_{33}^{im})$$

$$\sigma_{33}^{F} = 2C_{3311}^{*}(\epsilon_{11}^{A} + \epsilon_{11}^{C} + \epsilon_{11}^{im}) + C_{3333}^{*}(\epsilon_{33}^{A} + \epsilon_{33}^{C} + \epsilon_{33}^{im})$$

where, for ϵ_{ij}^{A}

$$\epsilon_{11}^{A} = -\nu\sigma_0/E$$

$$\epsilon_{33}^{A} = \sigma_0/E$$

for ϵ_{ij}^{C}

$$\epsilon_{11}^{C} = (S_{1111} + S_{1122})\epsilon_{11}^{T} + S_{1133}\epsilon_{33}^{T}$$

$$\epsilon_{33}^{C} = 2S_{3311}\epsilon_{11}^{T} + S_{3333}\epsilon_{33}^{T}$$

for ϵ_{ij}^{im}

$$\epsilon_{11}^{im} = -v[(S_{1111} + S_{1122} - 1)\epsilon_{11}^{T} + S_{1133}\epsilon_{33}^{T}]$$

$$\epsilon_{33}^{im} = -v[2S_{3311}\epsilon_{11}^{T} + (S_{3333} - 1)\epsilon_{33}^{T}]$$

for ϵ_{ij}^{T}

$$\epsilon_{11}^{T} = (DF - BG)/(AD - BC)$$

$$\epsilon_{33}^{T} = (AG - CF)/(AD - BC)$$

$$A = [(S_{1111} + S_{1122})(1 - v) + v](C_{1111} + C_{1122} - C_{1111}^{*} - C_{1122}^{*}) + 2S_{3311}(1 - v)(C_{1122} - C_{1122}^{*}) - (C_{1111} + C_{1122})$$

$$B = S_{1133}(1 - v)(C_{1111} - C_{1111}^{*}) + [(S_{1133} + S_{3333})(1 - v) + v] \times (C_{1122} - C_{1122}^{*}) - C_{1122}$$

$$C = 2[(S_{1111} + S_{1122})(1 - v) + v](C_{1122} - C_{1122}^{*}) + 2S_{3311}(1 - v)(C_{1111} - C_{1111}^{*}) - 2C_{1122}$$

$$D = 2S_{1133}(1 - v)(C_{1122} - C_{1122}^{*}) + [S_{3333}(1 - v) + v](C_{1111} - C_{1111}^{*}) - C_{1111}$$

$$F = \epsilon_{11}^{A}(C_{1111}^{*} + C_{1122}^{*} - C_{1111} - C_{1122}) + \epsilon_{33}^{A}(C_{1122}^{*} - C_{1122})$$

$$G = 2\epsilon_{11}^{A}(C_{1122}^{*} - C_{1122}) + \epsilon_{33}^{A}(C_{1111}^{*} - C_{1111})$$

for S_{ijkl} [5, 8]

$$S_{1111} = S_{2222} = Q\xi + R\psi$$

$$S_{3333} = Q\eta + 2R(2\pi - \psi)$$

$$S_{1122} = S_{2211} = \tfrac{1}{3}Q\xi - R\psi$$

$$S_{1133} = S_{2233} = Q\zeta - R\psi$$

$$S_{3311} = S_{3322} = Q\zeta/\alpha^2 - 2R(2\pi - \psi)$$

$$S_{1212} = \ldots. = \tfrac{1}{3}Q\xi + R\psi$$

$$S_{2323} = \ldots. = S_{3131} = \ldots. = \tfrac{1}{2}Q\zeta\left(\frac{\alpha^2 + 1}{\alpha^2}\right) + \tfrac{1}{2}R(4\pi - \psi)$$

α; aspect ratio

$$\psi = 2\pi\frac{\alpha}{(\alpha^2 - 1)^{3/2}}\{\alpha(\alpha^2 - 1)^{1/2} - \ln[\alpha + (\alpha^2 - 1)^{1/2}]\}$$

$$\xi = \frac{1}{\alpha^2 - 1}(\pi\alpha^2 - \tfrac{3}{4}\psi)$$

$$\zeta = \psi - \tfrac{4}{3}\xi$$

$$\eta = \tfrac{4}{3}\pi - 2\zeta$$

$$Q = \frac{3}{8\pi(1 - \nu)}$$

$$R = \frac{1 - 2\nu}{8\pi(1 - \nu)}$$

References

1. V. R. RILEY, *J. Compos. Mater.* **2** (1968) 436.
2. H. FUKUDA and T. W. CHOU, *J. Mater. Sci.* **16** (1981) 1088.
3. M. TAYA, *J. Compos. Mater.* **15** (1981) 198.
4. P. T. CURTIS, M. G. BADER and J. E. BAILEY, *J. Mater. Sci.* **13** (1978) 377.
5. J. D. ESHELBY, *Proc. Roy. Soc.* **A241** (1957) 376.
6. T. MORI and K. TANAKA, *Acta Metall.* **21** (1973) 571.
7. K. TAKAHASHI, T. SAKAI and K. HARAKAWA, *J. Compos. Mater. Suppl.* **14** (1980) 144.
8. K. WAKASHIMA, *J. Jpn. Soc. Compos. Mater.* **2** (1976) 161 (in Japanese).

Received 21 April
and accepted 21 July 1983